Accepted Manuscript

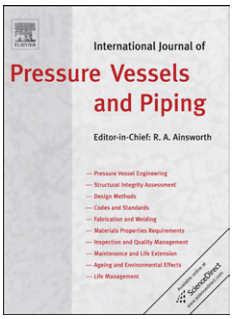

Title: Cold hydraulic expansion of oil well tubulars

Authors: A.R. Akisanya, F.U. Khan, W.F. Deans, P. Wood

PII: S0308-0161(11)00105-0

DOI: 10.1016/j.ijpvp.2011.08.003

Reference: IPVP 3137

To appear in: *International Journal of Pressure Vessels and Piping*

Received Date: 11 May 2010

Revised Date: 15 July 2011

Accepted Date: 10 August 2011

Please cite this article as: Akisanya AR, Khan FU, Deans WF, Wood P. Cold hydraulic expansion of oil well tubulars, International Journal of Pressure Vessels and Piping (2011), doi: 10.1016/j.ijpvp.2011.08.003

COLD HYDRAULIC EXPANSION OF OIL WELL TUBULARS

A.R. Akisanya[a,*], F.U. Khan[b], W.F. Deans[a] and P. Wood[b]

[a] School of Engineering, College of Physical Sciences,
King's College, University of Aberdeen, Aberdeen AB24 3UE, U.K.

[b] Read Well Services Limited, Viking House, 1 Claymore Avenue,
Offshore Technology Park, Aberdeen AB23 8GW, U.K.

ABSTRACT

The cold hydraulic expansion of two concentric tubulars is analysed with emphasis on the applications to oil and gas casings. Theories of elasticity and plasticity are used to develop a model relating the hydraulic pressure, the geometric dimensions of the tubulars and the residual contact pressure between the pipes. Nonlinear finite element analysis is used to validate the theoretical results and to investigate the effects of end support conditions. Hydraulic expansion experiments are conducted on tubulars and the measured evolution of the deformation and residual contact pressure are compared with the corresponding theoretical predictions and finite element solutions. There is a good agreement between the experimental results and predictions from the theoretical analysis and numerical simulations. The implications of the results for the design of casing hangers and patch repairs of oil and gas tubulars are discussed.

Keywords
Expandable tubular; Hydraulic expansion; thick-walled cylinders; interference; residual stresses.

1. INTRODUCTION

The cold expansion of tubes has been used for many decades in the assembly and leak repair of heat exchangers in power generation, nuclear and process industries, see for example Middlebrooks et al. [1] and Allam et al. [2]. In the assembly of many shell and tube heat exchangers, holes are drilled in the tube-sheet and a tube is placed in each of the holes. The tube is then plastically expanded onto the tube-sheet using either mechanical rolling method or hydraulic pressure. The interference fit that develops between the tube

and the tube-sheet upon unloading must provide a leak-proof joint between them. A similar expansion method is also used in the process industry to repair badly corroded tubes in heat exchangers. Here a new thin-walled tube (sometimes referred to as a sleeve) is inserted inside the existing tube bridging across the degraded section. The new tube is then cold expanded onto the existing tube, thereby eliminating the leak path. In these applications, the expansion is usually carried out over a relatively short length of the tube (between 25 mm to 50 mm) with the primary aim of providing a good leak-proof joint. The post-expansion structural and mechanical response is usually not a major concern since the joint is not load bearing in service.

The use of cold expanded tubulars in the oil and gas industry started just over a decade ago, driven mainly by the need to reduce drilling and completion costs and to explore deeper hydrocarbon reserves [3]. Recent applications of expandable technology in the industry include the cold expansion of production tubing, expandable sand screens, cladding or patching systems, expandable liner hangers and multilateral junctions; some of these applications are illustrated in Figure 1.

In contrast to the application to heat exchangers, the cold expansion of tubulars in the oil and gas industry is subject to many technical and operational challenges. The expansion is carried out *in-situ* downhole in an oil or gas well at a depth of several thousands metres, and the level of expansion can be up to 30% with an expanded length of pipe of up to 600 m (or more). In addition, the expanded tubular must withstand the downhole loading and environmental conditions, e.g. pressure of up to 150 MPa, temperature of up to 200 ^{o}C and the presence of a potentially corrosive environment. Consequently, the design of the deployment tools and the assessment of the post-expansion behaviour are technically more challenging. There is therefore an urgent need for detailed understanding of the inter-relationship between the expansion method, material selection, geometric parameters, and post-expansion mechanical response and corrosion characteristics of cold expanded tubulars before the technology can be fully accepted in the high costs and high risk environment as found in the oil and gas industry.

* Corresponding author. Email: a.r.akisanya@abdn.ac.uk. Tel.: +44 1224 272989. Fax: +44 1224 272497.

Some of these relationships are beginning to emerge, and recent efforts have focused on the development of expansion tools and means of downhole deployment. Three different methods currently exist for performing the expansion *in-situ* in an oil or gas well. These include: (i) roller cone tools whereby a radially expanding tool is rotated and pulled simultaneously through the pipe causing the pipe to expand, (ii) solid cone tools which are hydraulically and/or mechanically pulled (or pushed) through the pipe [4], and (iii) hydraulic expansion [5]. The choice of expansion method depends on the operational requirements. Both the roller and solid cone expansion methods are strain-controlled and have greater maximum achievable diametrical expansion than the hydraulic method, which is stress-controlled [4]. The hydraulic expansion method is considered in this paper.

The applications of the cold expansion of tubulars in the oil industry can be grouped into two main classes: internal tubing patch and external casing patch. In the internal tubing patch, the patch tubular is deployed into the oil or gas well to the depth at which it is to be set. The patch is then plastically expanded or swaged into contact with the outer casing using one of the three methods mentioned above; an interference fit is generated between the pipes upon unloading. This technique is well suited for a range of applications; for example, water shut off, repair of damaged tubing, and for isolation of perforated zones (see Figure 1). The external casing patch however is used for reconnecting casing string downhole. If a casing has been damaged (e.g. due to corrosion or wear) and its pressure rating is compromised then it may need to be replaced. The casing string below the damage will most likely be cemented in place and therefore not free to be removed. The section of the casing above the damage is removed by mechanical backoff at a threaded coupling or by cutting and subsequent pulling out of the well. A new casing is run over the outer diameter of the remaining casing allowing for an overlap between the two casings, and the old casing is then expanded onto the casing patch, thereby reconnecting a new length of casing which can now be “tied off” at surface.

The two applications described above involve the expansion of an inner pipe onto an outer pipe; this is sometimes referred to as swaging. The outer pipe for the internal tubing patch (and the inner pipe for the external casing patch) may be corroded, damaged or perforated, and thus the material and geometric dimensions of the patch tubular (and of the external casing patch) must be appropriately chosen to ensure adequate connection strength between the two pipes.

Liu et al [6] presented an elastic – plastic analysis of the hydraulic expansion of concentric tubulars. However, the analysis, which is based on strain compatibility between the tubulars, neglects the effects of the initial radial clearance between the tubulars on the residual contact pressure.

In the current paper, the mechanics of hydraulic expansion of tubulars are examined. Elastic/plastic analysis of the expansion process is carried out to determine the effects of material properties, geometric dimensions (including the initial radial clearance) and the swage pressure on the post-expansion interface or contact pressure between the pipes. The effects of the end support conditions on the expansion process are examined by nonlinear finite element analysis. Hydraulic expansion experiments are conducted using full-size typical oil well tubulars and the results are compared with predictions from the finite element and theoretical analyses.

2. ANALYSIS OF STRESS AND STRAIN DURING HYDRUALIC EXPANSION OF TUBULARS

Let us consider the hydraulic expansion of an internal pipe (referred to as pipe 1) onto an external pipe (referred to as pipe 2). The internal pipe is concentrically placed inside the external pipe such that a radial clearance δ exits between the pipes, see Figure 2. The internal pipe 1 has inner radius r_i and outer radius r_o; the corresponding radii for the external pipe 2 are denoted by R_i and R_o. For the internal tubing patch, the actual dimensions of the outer pipe may not be known but estimated values can be obtained from specialised cased-hole inspection tool.

The inner surface of the internal pipe 1 is pressurised using, for example, water, to swage or plastically expand a length of the internal pipe against the external pipe 2; the pressure is bled off after attaining a maximum swage pressure P_{smax}. In the following we shall provide the relationship between the applied swage pressure and the post-expansion interface (or contact) pressure between the two concentric pipes with given initial geometric parameters and material properties. The burst capacity of tubulars is not considered in this paper, but a detailed analysis of pre- and post-expansion burst capacity of tubulars under different end support conditions is available elsewhere; see for example Stewart et al. [7] and Klever and Stewart [8].

For simplicity, the following assumptions are made in the present analysis of the hydraulic expansion of tubulars.

(i) Both pipes are elastic/ideally-plastic with Young's modulus E, Poisson ratio ν and uniaxial yield strength Y_1 for pipe 1 and Y_2 for pipe 2.

(ii) The pipes are assumed to be isotropic, and the magnitude of the residual stresses developed after unloading from the maximum swage pressure is relatively small that Bauschinger effects on the deformation can be neglected. However, Bauschinger effects are important in assessing the post-expansion collapse response of the pipes [9].

(iii) The constraint on the axial movement of the pipes is small and thus the axial (or longitudinal) stress $\sigma_z \cong 0$.

(iv) Plastic yielding of pipe 1 occurs according to Tresca's yield criterion.

(v) The deformation of pipe 2 remains within the elastic limit during the swaging process.

The deformation of the pipes can be divided into four stages: elastic deformation of pipe 1; elastic/plastic deformation of pipe 1; post-contact deformation of pipes 1 and 2; and the deformation of pipes 1 and 2 during depressurisation. In the following we summarise the relationship between the applied swage pressure and the deformation (as characterised by the radial displacement or the hoop strain) for each stage of the deformation.

The elastic in-plane stresses and corresponding displacements in a thick-walled cylinder subjected to a combination of internal pressure P_{int} and external pressure P_{ext} are well-known, and are given by [10, 11]

$$\begin{aligned}
\sigma_r &= \frac{P_{int}}{k^2-1}\left(1-\frac{r_o^2}{r^2}\right)-\frac{k^2P_{ext}}{k^2-1}\left(1-\frac{r_i^2}{r^2}\right)\\
\sigma_\theta &= \frac{P_{int}}{k^2-1}\left(1+\frac{r_o^2}{r^2}\right)-\frac{k^2P_{ext}}{k^2-1}\left(1+\frac{r_i^2}{r^2}\right)\\
u &= \frac{P_{int}r}{E\left(k^2-1\right)}\left[(1-\nu)+(1+\nu)\frac{r_o^2}{r^2}\right]-\frac{k^2P_{ext}r}{E\left(k^2-1\right)}\left[(1-\nu)+(1+\nu)\frac{r_i^2}{r^2}\right]
\end{aligned} \tag{1}$$

where σ_r and σ_θ are the radial and hoop stresses respectively, u is the radial displacement, r_i and r_o are respectively the internal and external radii, $k = r_o/r_i$, r is the radial coordinate, and E and ν are respectively the Young's modulus and Poisson ratio of the material.

Stage I – Elastic deformation of pipe 1

During the initial stages of the pressurisation, the deformation of the internal pipe (pipe 1), which is subjected to an internal pressure P_s, is linear elastic, and there is no deformation of pipe 2 since the two pipes are not yet in contact. From (1), the in-plane stresses, hoop strain and the radial displacements at the outer surface of pipe 1 are

$$\sigma_{ro} = 0; \qquad \sigma_{\theta o} = \frac{2P_s}{k^2 - 1}; \qquad \varepsilon_{1o} = r_o u_o = \frac{2P_s}{E\left(k^2 - 1\right)} \tag{2}$$

and the corresponding stresses and hoop strain at the inner surface of the pipe are

$$\sigma_{ri} = -P_s; \qquad \sigma_{\theta i} = \frac{\left(k^2 + 1\right)P_s}{k^2 - 1}; \qquad \varepsilon_{1i} = r_i u_i = \frac{P_s\left[\left(k^2 + 1\right) + \nu\left(k^2 - 1\right)\right]}{E\left(k^2 - 1\right)} \tag{3}$$

where subscripts i and o refer to inner and outer surfaces respectively, and the other parameters are as defined earlier. The relationship between the applied pressure P_s and the hoop strain at the outer surface of pipe 1, ε_{1o}, is shown schematically in Figure 3; the initial elastic deformation is identified by curve 0-1 in the figure.

Stage II – Elastic/plastic deformation of pipe 1

The magnitude of the stresses in the pipe increases with increasing swage pressure until plastic yielding starts at the inner surface of the pipe. Using Tresca's yield criterion and the stresses given in (3), it can be shown that plastic yielding starts at an applied swage pressure of magnitude

$$P_s = P_y = \frac{Y_1\left(k^2 - 1\right)}{2k^2} \tag{4}$$

where Y_1 is the uniaxial yield strength of the material from which the pipe is made.

Further increase in the pressure beyond the yield pressure given by (4) results in the spread of the plastic deformation towards the outer surface of the pipe. By solving the stress equilibrium equation and making use of Tresca's yield criterion, the pressure at which

plastic deformation occurs across the whole wall thickness of the pipe (sometimes referred to as the ultimate or limit pressure) is obtained as [10]

$$P_s = P_p = Y_1 \ln k \,. \tag{5}$$

For an elastic/ideally-plastic material as assumed in the present study, or for materials whose rate of hardening is of the order of the yield stress, a slight increase in the pressure above the ultimate pressure given by (5) is sufficient to produce strains of appreciable magnitude. Thus, once the ultimate pressure (5) is attained, significant plastic deformation occurs at almost a constant pressure until pipe 1 makes contact with pipe 2; this deformation process is identified as curve 2-3 in Figure 3. This significant plastic deformation may lead to strain localisation and necking before pipe 1 makes contact with pipe 2; this must be avoided in practice.

The engineering hoop strain at the onset of localisation for a circular pipe subjected to an internal pressure has been shown to be $\{\exp(n/2)-1\}$, where n is the strain hardening index of the material from which the pipe is made; $n \cong 0.15$ for duplex stainless steel, $n \cong 0.2$ for low carbon steel, and $n \cong 0.5$ for austenitic stainless steel [4, 7,8]. For a pipe made from low carbon steel, the strain at the onset of localisation is about 10%. Although material strain hardening is not considered in the present analysis, a comparison between the hoop strain at the onset contact (i.e. $\varepsilon_{1c} = \delta/r_o$) and the predicted localisation hoop strain can be used to determine the maximum allowable radial clearance δ between the tubulars.

Stage III – Post contact deformation of pipes 1 and 2

Once contact is made with the outer pipe 2 (identified as point 3 in figure 3), an interface pressure P_c develops at the contact surface between the pipes due to the constraint which pipe 2 imposes on the deformation of pipe 1. The swage pressure must therefore increase to ensure further plastic deformation of pipe 1. The inner pipe 1, which is fully plastic, is now subjected to an internal swage pressure of magnitude

$$P_s = P_c + P_p = P_c + Y_1 \ln k \,, \tag{6}$$

and an external pressure of magnitude P_c, while pipe 2 is simultaneously subjected to an internal pressure of P_c, as illustrated in Figure 4.

The maximum allowable interface pressure P_c (= P_{cy}) for pipe 2 to remain elastic during the swaging process, which is one of the assumptions, can be determined in the same manner as for pipe 1 (see eqn. (4)), and it is given by

$$P_{cy} = \frac{Y_2\left(K^2 - 1\right)}{2K^2}, \tag{7}$$

where Y_2 is the uniaxial yield strength of the material from which pipe 2 is made, and $K = R_o/R_i$, where R_o and R_i are respectively the outer and inner radii of pipe 2. Consequently, the maximum allowable swage pressure, P_{smax}, before de-pressurisation must satisfy the relation

$$P_p < P_{smax} \le (P_{cy} + P_p) \tag{8}$$

to avoid plastic deformation of pipe 2, where P_p is the ultimate pressure for pipe 1.

The stresses, strains and radial displacement in pipe 2 during the expansion can be obtained by using eqn. (1) for a circular cylindrical pipe subjected to an internal pressure $P_{int} = P_c$ and external pressure P_{ext} = 0. The hoop strain ε_{2o} at the outer surface and the corresponding radial displacement U_i at the inner surface of pipe 2 during loading are therefore given by

$$\varepsilon_{2o} = \frac{2\left(P_s - P_p\right)}{E\left(K^2 - 1\right)} \tag{9}$$

$$U_i = \frac{R_i\left(P_s - P_p\right)}{E\left(K^2 - 1\right)}\left[\left(K^2 + 1\right) + \nu\left(K^2 - 1\right)\right] \tag{10}$$

Recall that the swage pressure $P_s > P_p$ after the onset of contact.

Pipe 1 remains fully plastic as the swage pressure is increased after the initial contact with pipe 2, and the radial displacement of the outer surface of pipe 1 increases by a magnitude U_i, given in eqn. (10). The total hoop strain ε_{1o} at the outer surface of pipe 1 at a given swage pressure P_s (> P_p) is therefore $(\delta + U_i)/r_o$, where δ is the initial radial clearance between the pipes. This total strain is a combination of the plastic and elastic (i.e. recoverable) strains. The plastic strain is not considered here, since the focus of this paper

is on the determination of the interface pressure after unloading. The P_s versus ε_{1o} relation after contact is shown schematically as curve 3-4 in Figure 3.

Since pipe 1 is subjected to a combination of internal pressure P_s (> P_p) and external pressure P_c after contact with pipe 2, the elastic radial displacement at the outer surface of pipe 1 during this stage of the deformation is therefore

$$\bar{u}_o = \frac{2r_o P_s}{E\left(k^2-1\right)} - \frac{r_o P_c}{E\left(k^2-1\right)}\left[\left(k^2+1\right)-\nu\left(k^2-1\right)\right] \tag{11}$$

where $P_c = 0$ if $P_s \le P_p$.

Stage IV – Deformation of the pipes during unloading

After reaching a chosen maximum swage pressure P_{smax}, the system is completely depressurised. The choice of the maximum pressure will depend on the expected level of expansion for the particular application of the process. The interface pressure just before unloading is P_{cmax} (= $P_{smax} - P_p$), and the corresponding elastic displacement of the inner surface of pipe 2, U_{imax}, is obtained by substituting P_{smax} into eqn. (10).

Let the instantaneous swage pressure and the corresponding interface pressure between the two pipes during the unloading be P_{su} and P_{cu}, respectively. We assume that both pipes unload in a linear elastic manner. The interface pressure depends on the relative elastic displacement recovery at the contacting surfaces, i.e. $R_i\varepsilon_{2rec} - r_o\varepsilon_{1rec}$, where ε_{1rec} and ε_{2rec} are the elastic hoop strains at the contacting surfaces of the pipes (see Figure 3). Thus, a reduction of the swage pressure from P_{smax} to P_{su} will reduce the elastic radial displacement at the outer surface of pipe 1 by a magnitude $\Delta\bar{u}_o$ given by

$$\Delta\bar{u}_o = \frac{2r_o\left(P_{s\max} - P_{su}\right)}{E\left(k^2-1\right)} - \frac{r_o\left(P_{c\max} - P_{cu}\right)}{E\left(k^2-1\right)}\left[\left(k^2+1\right)-\nu\left(k^2-1\right)\right], \tag{12}$$

while the elastic radial displacement at the inner surface of pipe 2 should reduce by a magnitude ΔU, given by

$$\Delta U = \frac{R_i\left(P_{c\max} - P_{cu}\right)}{E\left(K^2-1\right)}\left[\left(K^2+1\right)+\nu\left(K^2-1\right)\right] \tag{13}$$

These two displacements must be equal to ensure the two pipes remain in contact during the unloading. Equality of (12) and (13) gives the interface pressure P_{cu} during the depressurisation as

$$P_{cu} = \left[\frac{Q\left(k^2-1\right)-2}{Q\left(k^2-1\right)}\right]P_{s\,max} - Y_1 \ln k + \frac{2P_{su}}{Q\left(k^2-1\right)} \tag{14}$$

where

$$Q = \left(1-\frac{\delta}{R_i}\right)^{-1}\left[\frac{\left(K^2+1\right)+\nu\left(K^2-1\right)}{K^2-1}\right] + \left[\frac{\left(k^2+1\right)-\nu\left(k^2-1\right)}{k^2-1}\right]. \tag{15}$$

In eqns. (14) and (15), P_{smax} is the maximum swage pressure just before unloading, P_{su} is the instantaneous swage pressure during unloading, δ is the initial radial clearance between the pipes, r_o is the initial outer radius of pipe 1, and k and K are respectively the ratio of the outer radius to the inner radius for pipes 1 and 2. The corresponding hoop strain at the outer surface of pipe 2 during unloading is therefore

$$\varepsilon_{2u} = \frac{2P_{cu}}{E\left(K^2-1\right)} \tag{16}$$

Note that the instantaneous interface pressure during unloading P_{cu} depends on the instantaneous swage pressure P_{su} as given by eqn. (14).

After complete depressurisation, P_{su} = 0, and P_{cu} in eqn. (14) then becomes the residual interface (or contact) pressure between the pipes, P_{cr}, where

$$P_{cr} = \left[\frac{Q\left(k^2-1\right)-2}{Q\left(k^2-1\right)}\right]P_{s\,\max} - Y_1 \ln k \ . \tag{17}$$

The analysis presented above for open-ended pipes and based on Tresca yield criterion is also valid for von Mises yield criterion as the pressure at full plasticity $P_b = Y_1 \ln(k)$ for both criteria. Thus, the predicted fully plastic pressure (5) and the residual interface pressure (17) are valid for both Tresca and von Mises yield criteria provided the pipes are open-ended. However for closed-ended pipes, eqn (17) is only valid for Tresca yield criterion, and while for von Mises criterion the yield stress Y_1 for pipe 1 must be multiplied by a

factor of $2/\sqrt{3}$. Klever and Stewart [8] have shown that the average of the burst pressure predicted by Tresca and von Mises criteria is an unbiased predictor of the actual burst pressure; the same can be said for the fully plastic pressure. Therefore, for closed-ended pipes, a more accurate prediction of P_p and P_{cr} based on the average of the Tresca and von Mises predictions can be obtained by multiplying the yield stress Y_1 by the factor $\frac{1}{2}\left(1+\frac{2}{\sqrt{3}}\right)=1.08$ in eqns. (5) and (17). Thus, the residual interface pressure predicted by (17) would be greater for open-ended pipes than for closed-ended pipes.

The analysis of hydro-forming of double layered tubes by Liu et al. [6] suggested the use of hoop strain compatibility between the tubes to determine the residual interface pressure. However, the analysis neglects the strain accumulated in the inner pipe (Pipe 1) just before contact is made with the outer pipe (Pipe 2). Consequently, the relationship between the swage pressure and the residual interface (or contact) pressure provided by Liu et al. [6] (see eqn. (18) of Liu et al. [6]) is independent of the initial radial clearance between the pipes. The hoop strain in pipe 1 is in general not equal to the hoop strain in pipe 2 because pipe 1 is pre-strained before contact is made with pipe 2; the level of pre-strain depends on the initial radial clearance between the pipes. The strain in pipe 1 at the instance of first contact with the pipe 2 may be dominated by significant plastic deformation and this has a major effect on the residual interface pressure.

The use of the hoop strain compatibility as suggested by Liu et al. [6] may be suitable for tubes which are initially in contact before the expansion process commences or which have relatively insignificant initial radial clearance, as usually found in the patch repair of heat exchanger tubes, where the plastic strain in the inner pipe just before contact with the outer pipe is kept below about 1% [12]. Such an approach may, however, not be suitable for the expansion of tubulars for applications where the internal pipe 1 is subject to significant hoop strain, as found, for, example, in some applications in the oil industry where the maximum hoop strain during the expansion process may be as high as 25%. The method of relative elastic displacement between the pipes, as described in the present paper, is suitable for both scenarios of small and relatively large radial clearance.

3. NUMERICAL SIMULATIONS

Finite element analysis of the expansion process was carried out using ABAQUS CAE [13] to verify the analytical solution presented above and to examine the effects of other effects, such as the end constraint conditions. The inner and outer radii of the pipes used in the finite element simulation were r_i = 110 mm and r_o = 122 mm for the internal pipe 1, and R_i = 125 mm and R_o = 137 mm for the external pipe 2. Consequently, $k = r_o/r_i$ = 1.11, $K = R_o/R_i$ = 1.1, and the relative radial clearance δ/r_o = 0.0246. Both pipes were 3.05 m in length and arranged such that there was 2.44 m overlap between them, as shown in Figure 5a.

One end of each pipe was constrained to move only in the radial direction (see Figure 5a), while the other end was unconstrained, thus ensuring there was no constraint on the axial movement of the pipes. This boundary condition is referred to in this paper as "free ends". Mesh sensitivity test was carried out for a pipe subjected to an internal pressure by comparing the finite element prediction of the elastic stresses with the corresponding theoretical prediction given by eqn. (1). The finite element results using four eight-noded axisymmetric elements with reduced integration (CAX8R in ABAQUS) along the thickness direction was in agreement with the theoretical prediction to within 0.5%. Each pipe was therefore modelled with a total of 4,060 eight-node, two-dimensional axisymmetric elements with four elements in the thickness direction. Internal pressure during the swaging was applied incrementally on the inner surface of pipe 1 over a 1.59 m length as shown in Figure 5a, and then unloaded once the required maximum swage pressure was reached.

The simulation of the cold expansion process was carried out using J2 flow theory assuming an elastic/ideally-plastic solid. Recall that the fully plastic pressure and the residual interface pressure for open-ended pipes are independent of the yield criteria used: Tresca or von Mises (i.e. J2 flow theory). Both pipes had identical Young's modulus E = 210 GPa and Poisson ratio ν = 0.33, and uniaxial yield strength Y_1 = 702 MPa for pipe 1 and Y_2 = 980 MPa. The contact interaction between the pipes was modelled using a friction coefficient of μ = 0.25.

The deformed shape of the pipes after complete depressurisation is shown schematically in Figure 5b; the contact length of the pipe is slightly less than the pressurised length due to axial contraction and bending of the pipes, mostly of internal pipe 1. The numerically predicted residual interface (or contact) pressure after swaging to a pressure of P_s = 169 MPa is shown in Figure 6 as a function of distance along the contacting surfaces; the distance is measured from point A to D along the length of the pipe, as identified in Figure 5b. The interface pressure is nearly uniform along the contact length, with peaks in the interface pressure at either end of the contact length. Hereafter, the interface pressure will be reported as the average value over the contact length, excluding the peak values.

The evolution of the hoop strain at the outer surface of pipe 2 with the applied swage pressure P_s is shown in Figure 7. For each of the three different values of P_s considered, the deformation of pipe 2 started at an applied swage pressure of 76 MPa; this is the pressure at which the inner pipe 1 first made contact with the outer pipe 2. This is in reasonable agreement with the predicted value of $Y_1 \ln k$ = 73 MPa.

Further increase in the swage pressure resulted in the elastic deformation of the outer pipe 2 until plastic yielding commenced in pipe 2 at a swage pressure of 154 MPa. This compares favourably with the theoretically predicted swage yield pressure for pipe 2 of magnitude 152 MPa, see eqns. (7) and (8). We note that the magnitude of the residual hoop strain at the outer surface of pipe 2 and the corresponding residual interface pressure increase with increasing maximum swage pressure before depressurisation.

One of the assumptions of the theoretical analysis was that the outer pipe 2 must remain elastic during the swaging process. In order to compare the theoretical prediction of the pressure versus hoop strain response with the corresponding finite element solution, a swage pressure less than yield pressure for pipe 2 (= 154 MPa) must be used in the finite element simulation. A comparison between the predictions from the analytical model and the finite element analysis at a maximum swage pressure of P_s = 145 MPa is shown Figure 8. There is a very good agreement between the theoretical and finite element predictions during loading and unloading for the swage pressure versus hoop strain response of pipe 2 (Figure 8a), and also the swage pressure versus interface pressure

response (Figure 8b). We conclude that the theoretical model adequately describes the response of the pipes during the loading and unloading phases of the hydraulic expansion.

Additional numerical simulation was carried out to investigate the effects of end support conditions on the swaging process and residual interface pressure. The cold expansion of tubulars in oil and gas wells usually involve the use of relatively large elastomeric seals (usually referred to as packers), and the external tubulars (mainly casings) may be cemented in place. These will therefore restrict the axial movement of the pipes during the expansion. The results presented above are for pipes with no axial constraint. In this additional simulation, the ends of the two pipes were constrained against axial movement; this is referred to as "fixed ends". For the fixed ends, axial tension develops as the swaging process progresses; the magnitude of the axial tension will increase with increasing swage pressure. Plastic yielding of the internal pipe 1 is therefore dependent on both the applied pressure and the axial tension. The distribution of the residual interface pressure along the contact length is qualitatively similar for both the "fixed ends" and the "free ends", as shown in Figure 6. The average residual interface pressure at the same maximum swage pressure before depressurisation is 14 MPa for the "fixed end" and 16 MPa for the "free ends". The greater value of the fully plastic pressure for closed-ended pipes in comparison to open-ended pipes as discussed earlier leads to a lower residual interface pressure for closed-ended pipes. Thus, the constraint on the axial movement due to the seals and cementing of the casings slightly reduces the residual interface pressure at a given maximum swage pressure.

4. EXPERIMENTS

Swaging experiments were carried out on oil well steel tubulars to validate the theoretical and numerical predictions. The internal pipe 1 was a L80 grade tubular with inner radius of r_i = 110 mm and outer radius of r_o = 122 mm (i.e. $9\frac{5}{8}$-inch OD), while the external pipe 2 was a P110 grade casing with inner radius of R_i = 125 mm and outer radius of R_o = 137 mm (i.e. $10\frac{3}{4}$-inch OD). Thus the initial radial clearance was δ = 3 mm.

Uniaxial tensile samples were machined from the pipes in the hoop direction and tested; representative uniaxial stress-strain responses are shown in Figure 9. The uniaxial yield stress was 640 MPa for the L80 and 897 MPa for P110, and the ultimate tensile strength

(UTS) was 764 MPa for L80 and 1063 MPa for P110. The level of strain hardening was small in the material from which the pipes were made.

The length of each of the pipes tested was 3.05 m, and the L80 pipe was inserted inside the P110 pipe ensuring the pipes were concentrically placed, with an overlapping axial length of 2.4 m between the two pipes. An axial length 1.65 m within the overlapping region was isolated for expansion by elastomeric seals. Three strain gauges were mounted on the external surface of the outer pipe to measure the hoop strain during the swaging operation. One of the gauges was placed mid-way between the seal locations, while each of the other two gauges was placed at a distance of 413 mm from the centrally placed gauge. A schematic diagram of the experimental setup is shown in Figure 10. The swage pressure was applied in increments using a hydraulic pump until a pressure of 145 MPa was attained, and the system was then depressurised. The hoop strains and the swage pressure were continuously monitored and recorded using a computerised data logger.

The experimentally measured swage pressure versus hoop strain response for pipe 2, and the swage pressure versus interface pressure response are compared with the corresponding theoretical and the finite element predictions in Figure 8. The finite element results shown in Figure 8 were obtained by assuming the pipes were made from an elastic-ideally plastic material, with a yield strength which is the average of the initial yield strength and the UTS as obtained in the uniaxial tensile test: Y_1 = (640 + 764)/2 = 702 MPa for pipe 1, and Y_2 = (897 + 1063)/2 = 980 MPa for pipe 2. The experimental results from the hydraulic expansion indicate the internal L80 pipe came into contact with the external P110 pipe at a pressure of 71 MPa; this is in good agreement with the value of 76 MPa from the finite element simulation and a value of 73 MPa from the theoretical prediction.

The measured residual interface pressure was 8 MPa which is slightly less than 10.8 MPa from the theoretical model and the 11.5 MPa from the finite element analysis. There is therefore a very good agreement between the residual interface pressure predicted by the theoretical model and by the finite element simulation. The discrepancy between the measured residual interface pressure and the two predictions can be attributed to the fact that the model and the finite element simulations assumed elastic/ideally-plastic material while the materials from which the pipes were made do actually strain harden, though mildly. The level of deformation and the strains at a given swage pressure would therefore

be lower in the strain hardening pipes than for the corresponding elastic/ideally-plastic pipes, thereby reducing the interface pressure. Further, the seals used to contain the hydraulic fluid in the pipe do impose some constraint on the axial movement of the pipes, with a consequential effects of reducing the residual interface pressure at a given maximum swage pressure, see for example, Figure 6.

The solution of the residual interface pressure presented by Liu et al. [6] does not account for the effect of the initial radial clearance. Using the geometric and material parameters for the materials tested, the analysis of Liu et al. [6] predicts a residual interface pressure of 9.2 MPa; cf 8 MPa from the experiment, 10.8 MPa from current theoretical analysis and 11.5 MPa from finite element analysis. The discrepancy between Liu et al. [6] prediction and that from the current analysis is attributed to the initial radial clearance. The effect of the relative initial radial clearance δ/r_o on the residual interface pressure from the current analysis is shown in Figure 11; δ/r_o = 0.0245 in the experiment. The difference between the residual interface pressure predicted by Liu et al. [6] and that predicted from the current analysis increases with increasing value of the initial radial clearance.

5. CONCLUDING REMARKS

The hydraulic expansion of two concentric tubulars has been analysed and the pressure requirements have been determined as functions of the material properties and geometric dimensions. The predictions of the evolution of the deformation and residual interface pressure from the analytical model, which was based on the analysis of a thick-walled cylinder, compare favourably with those from non-linear finite element analysis and full-size hydraulic expansion experiments. The analysis presented in the paper is applicable to the hydraulic expansion of two concentric plain pipes for a wide range of applications, including the repair of heat exchanger tubes, and patch and cladding of oil and gas well production and completion tubulars and casings.

ACKNOWLEDGEMENTS

This work was funded as part of a KTP programme (Programme Number 4267). The authors are grateful to the UK Department for Business, Innovation and Skills (formerly Department of Trade and Industry) for financial support.

REFERENCES

[1] Middlebrooks WB, Harrod DL, Gold RE. Residual-stresses associated with the hydraulic expansion of steam-generator tubing into tubesheets, Nuclear Engineering and Design, 1993; 143: 159-169.

[2] Allam M, Chaaban A, Bazegui A. Optimum expansion and residual contact pressure levels of hydraulically expanded tube-to-tubesheet joints, Trans. Canadian Society for Mechanical Engineering, 1997; 21**:** 415-434.

[3] Filippov A, Mack R, Cook L, York P, Ring L, McCoy T. Expandable tubular solutions, Paper number SPE 56500, Proceedings of the SPE Annual Technical Conference and Exhibition, Houston, Texas, USA; 1999.

[4] Stewart RB, Marketz F, Lohbeck WCM. (1999). Expandable wellbore tubular, Paper number SPE 60766, Proceedings of the SPE Technical Symposium on Quest for Solutions in a Changing Industry, Dhahran, Saudi Arabia; October 1999.

[5] Louden F, Hazel P, Skjerping F, Gorrara A, Boe K. Development of a hydraulically expanded metal internal casing patch. Paper number SPE 94056-PP. Proceedings of the SPE/ICoTA Coiled Tubing Conference and Exhibition, The Woodlands, Texas, USA; 2005.

[6] Liu F, Zheng J, Xu P, Xu M, Zhu G. Forming mechanism of double-layered tubes by internal hydraulic expansion. International Journal of Pressure Vessels and Piping, 2004; 81: 625-633.

[7] Stewart G, Klever FJ, Ritchie D. An analytical model to predict the burst capacity of pipelines, Proceedings of the 13th International Conference on Offshore Mechanics and Artic Engineering, Houston, Texas, USA; 1994.

[8] Klever FJ, Stewart G. Analytical burst strength prediction of OCTG with and without defects, SPE Paper 48329, Proceedings of SPE Applied Technology Workshop on Risk-based Design of well Casing and Tubing, The Woodlands, Texas, USA; 1998.

[9] Mack R, Filippov A, Kendziora L, Ring L. In-situ expansion of casing and tubing – effect on mechanical properties and resistance to sulphide stress cracking, Paper number 164, NACE International Corrosion Conference, Houston Texas, USA; 2000.

[10] Ugural AC, Fenster SK. Advanced Strength and Applied Elasticity, 3rd ed., New Jersey: Prentice-Hall PTR; 1995.

[11] Chakrabarty J. Theory of Plasticity, New York: McGraw-Hill; 1987.

[12] Bourouga B, Bardon JP. Thermal contact resistance at the interface of double tubes assembled by plastic deformation. Experimental Thermal and Fluid Science, 1998; 18: 168-181.

[13] ABAQUS CAE, Hibbitt, Karlsson and Sorensen, Inc. Pawtucket R.I., USA; 2005.

FIGURE CAPTIONS

Figure 1 Illustration of some applications of expandable tubular technology in the oil and gas industry.

Figure 2 A schematic diagram showing the configuration of the two concentric pipes, geometric parameters and the swage pressure.

Figure 3 Schematic of the loading and unloading response of (a) swage pressure P_s versus hoop strain ε_{1o} at the outer surface of internal pipe 1, and (b) swage pressure P_s versus hoop strain ε_{2o} at the outer surface of external pipe 2. The arrows indicate the directions of loading and unloading.

Figure 4 The cross-section of the pipes and, loading before and after contact.

Figure 5 (a) The configuration, dimensions (in mm) and boundary conditions used in the finite element simulation. (b) A schematic of the deformed shape obtained from the finite element analysis.

Figure 6 The variation of the post-expansion residual interface pressure along the contact length for two different end support conditions as predicted by the finite element analysis. The letters A to D relate to the points along the deformed shape as shown in Figure 5.

Figure 7 Finite element prediction of the evolution of the hoop strain at the outer surface of external pipe 2 with the swage pressure. The arrows in indicate the directions of loading and unloading.

Figure 8 Comparison of the predictions from the theoretical model, finite element analysis and full-size experiments for (a) swage pressure versus hoop strain response for pipe 2, and (b) swage pressure versus interface pressure relation. The arrows indicate the directions of loading and unloading.

Figure 9 The uniaxial stress – strain response in tension for L80 grade tubular and P110 casing.

Figure 10 A schematic diagram of the experimental setup of the hydraulic expansion of two concentric tubulars.

Figure 11 The effect of relative initial radial clearance on the residual interface pressure. The swage pressure was 145 MPa.

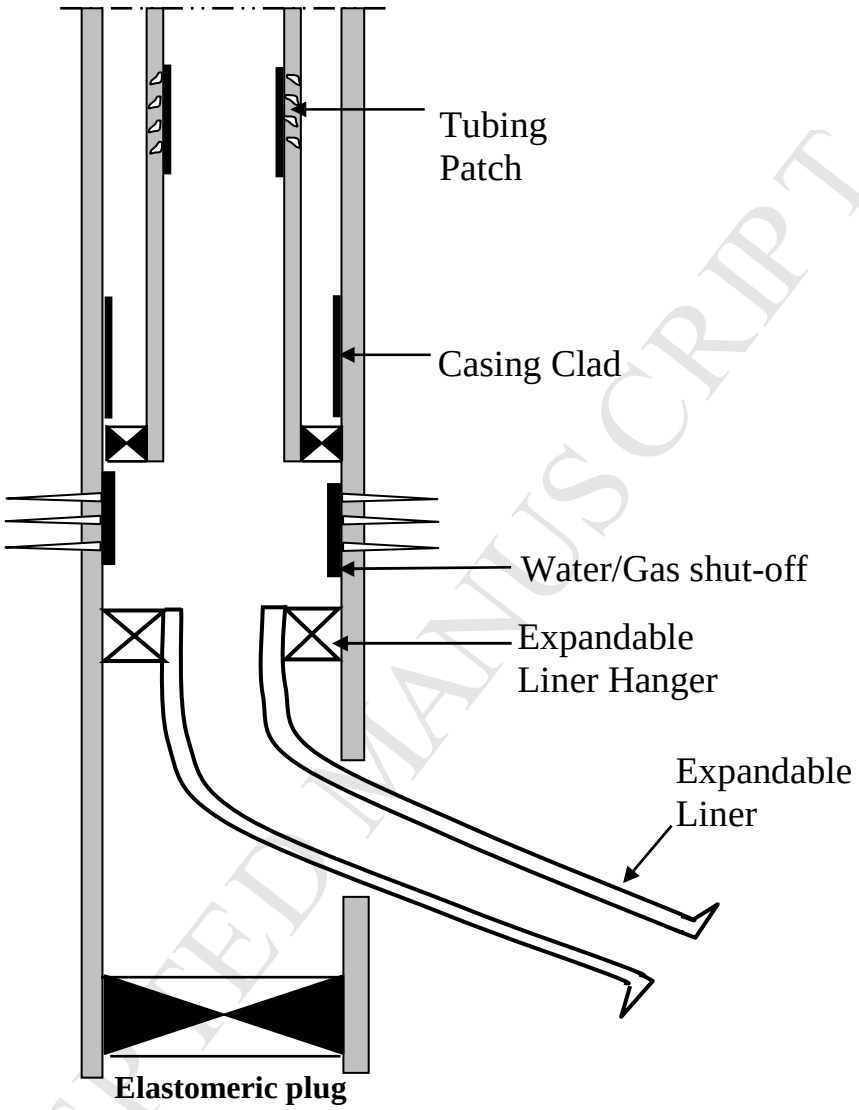

Figure 1

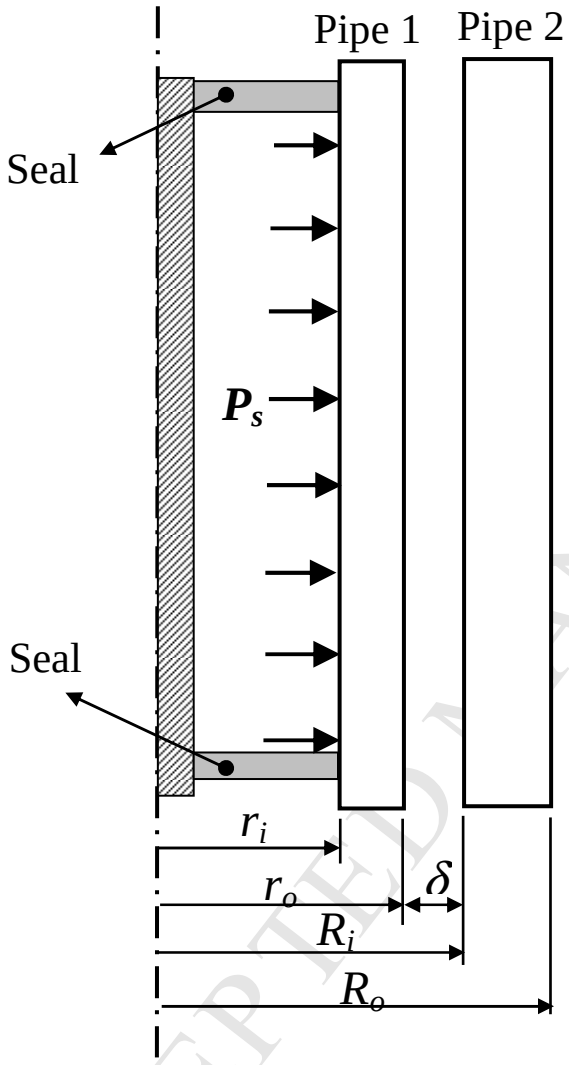

Figure 2

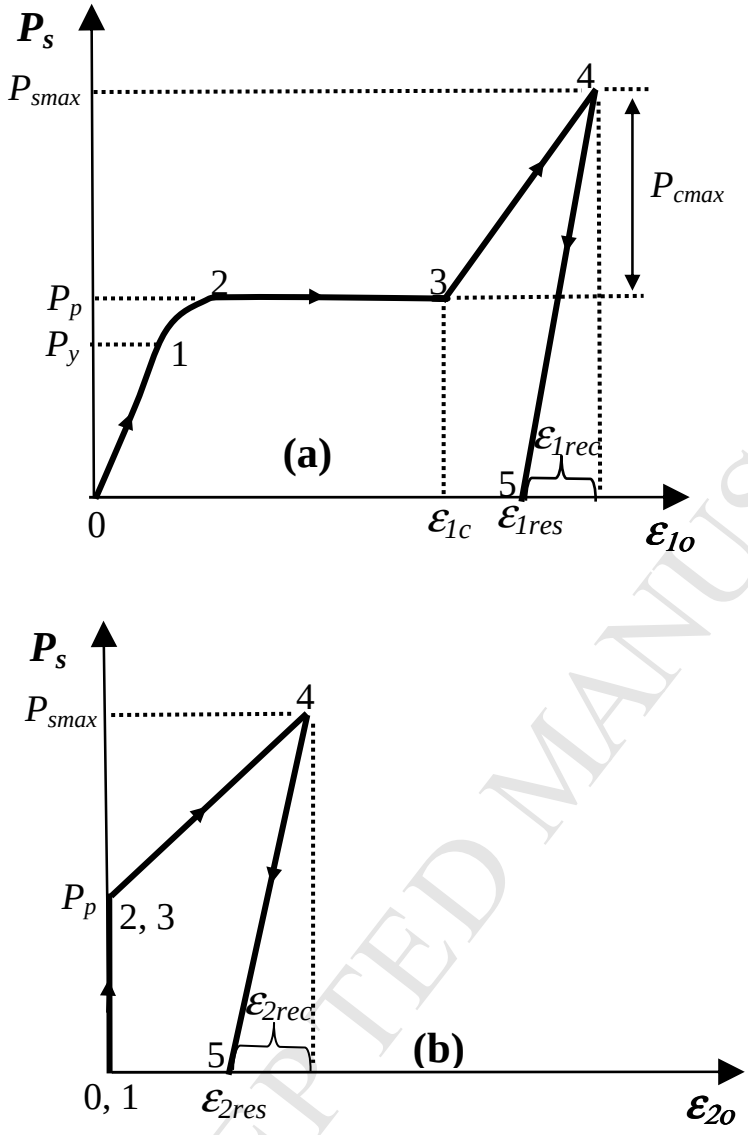

Figure 3

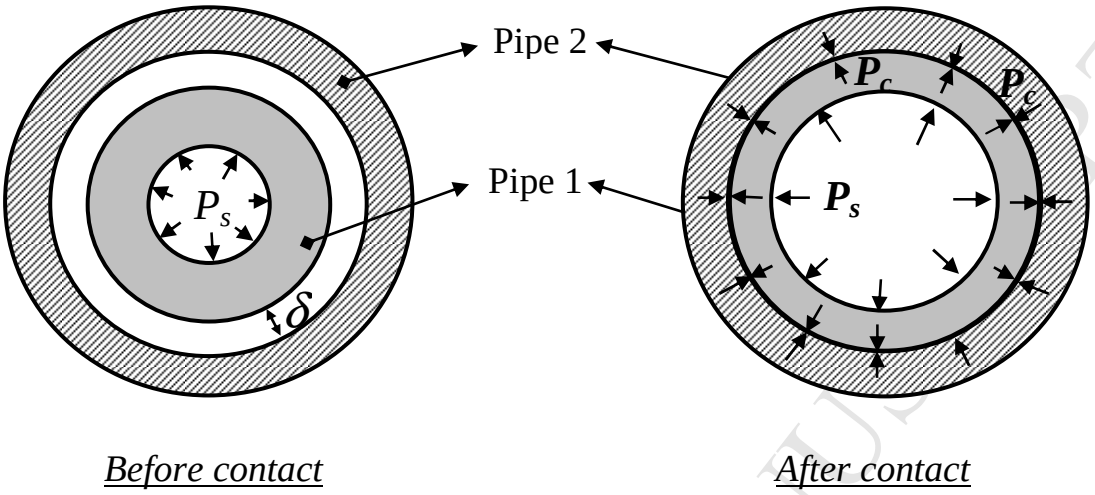

Figure 4

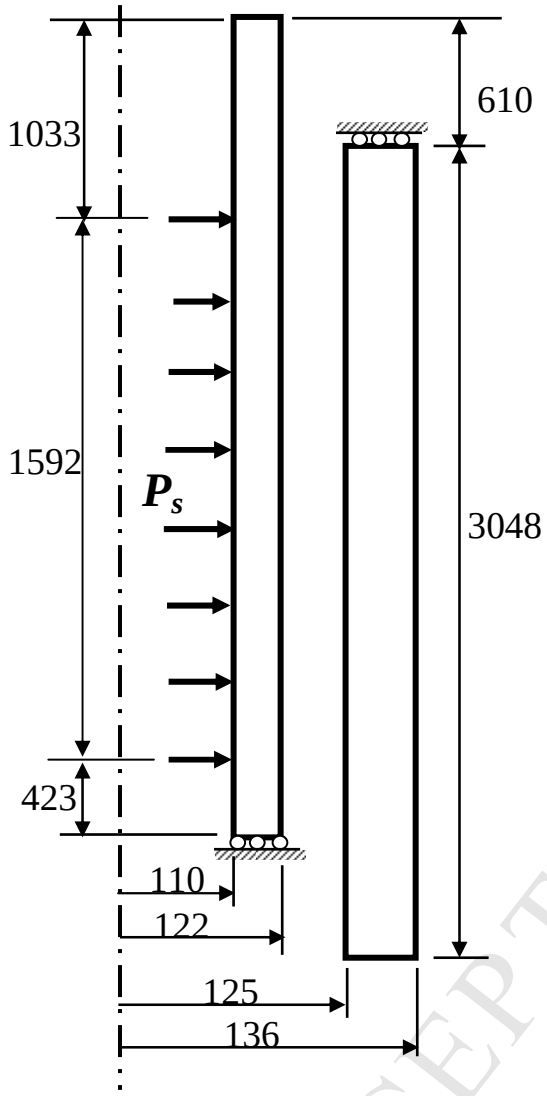

(a)

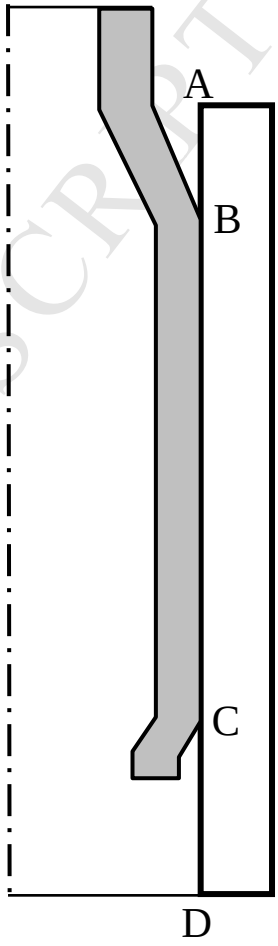

(b)

Figure 5

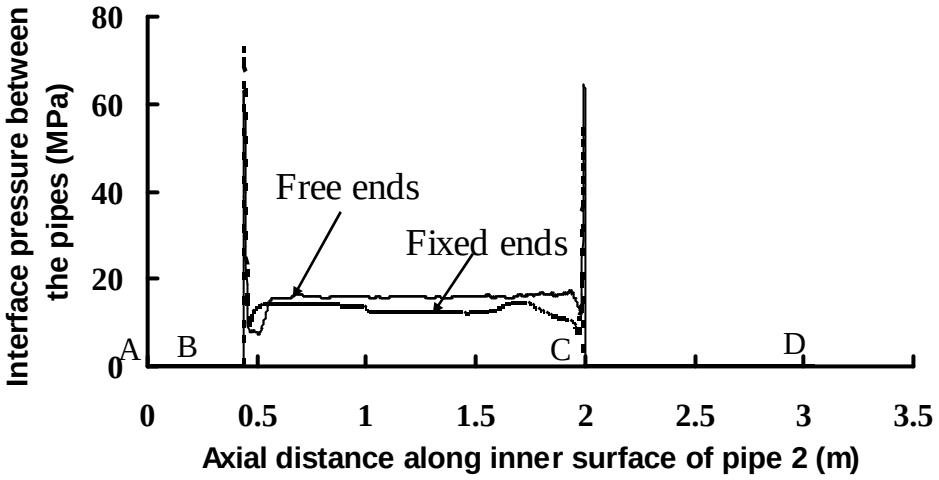

Figure 6

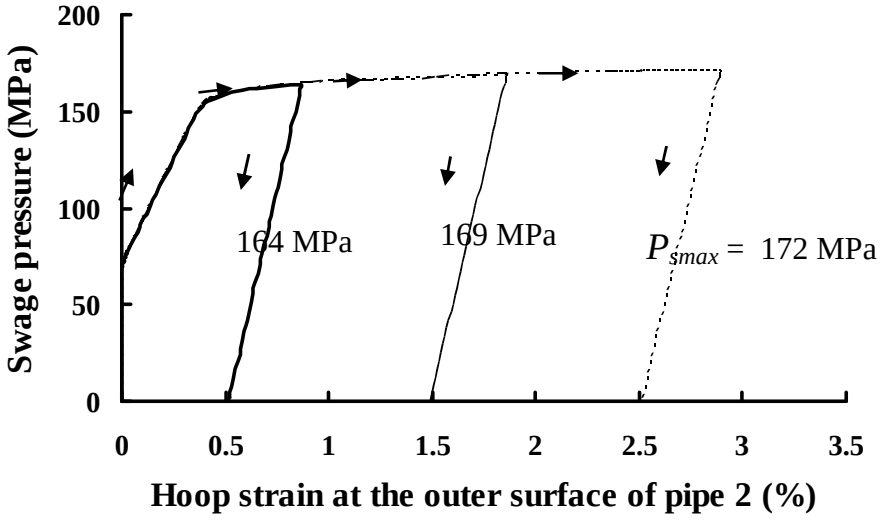

Figure 7

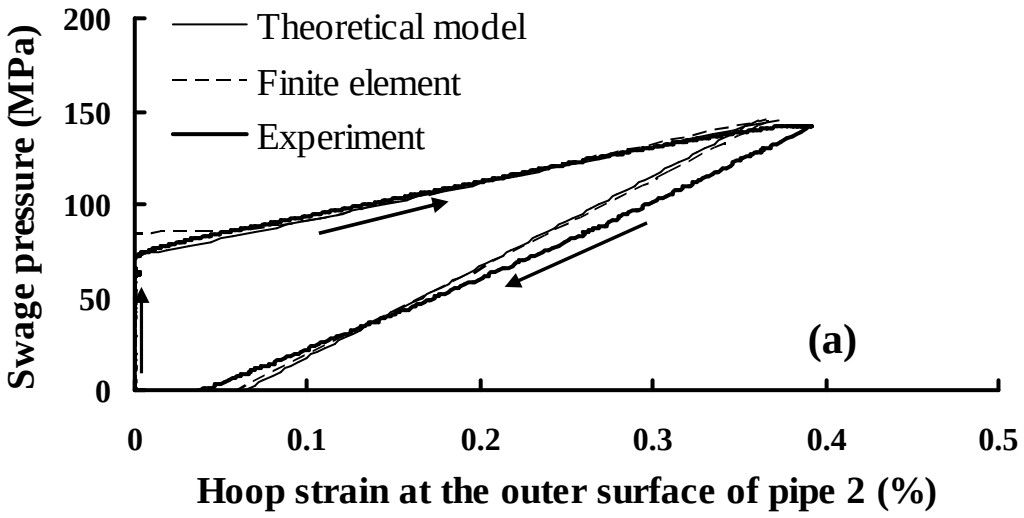
Theoretical model
Finite element
Experiment
Swage pressure (MPa)
200
150
100
50
0
0
0.1
0.2
0.3
0.4
0.5
(a)
Hoop strain at the outer surface of pipe 2 (%)

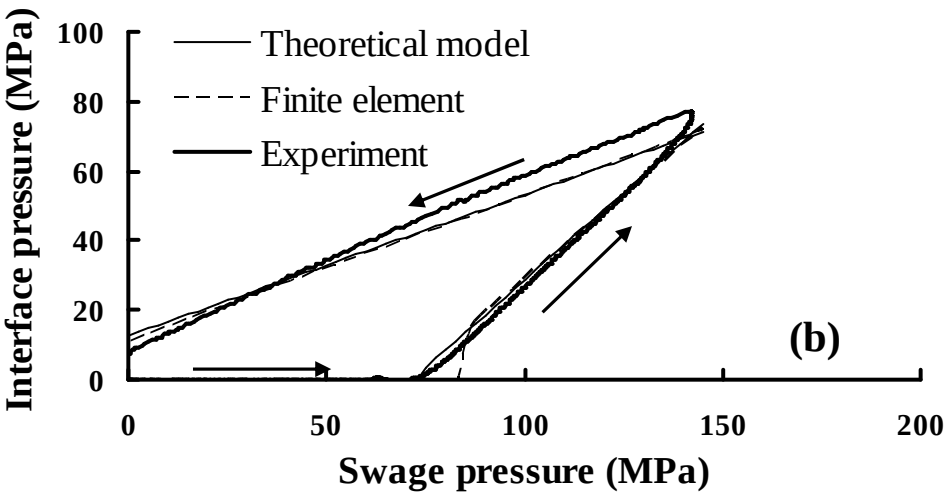
Theoretical model
Finite element
Experiment
Interface pressure (MPa)
100
80
60
40
20
0
0
50
100
150
200
(b)
Swage pressure (MPa)

Figure 8

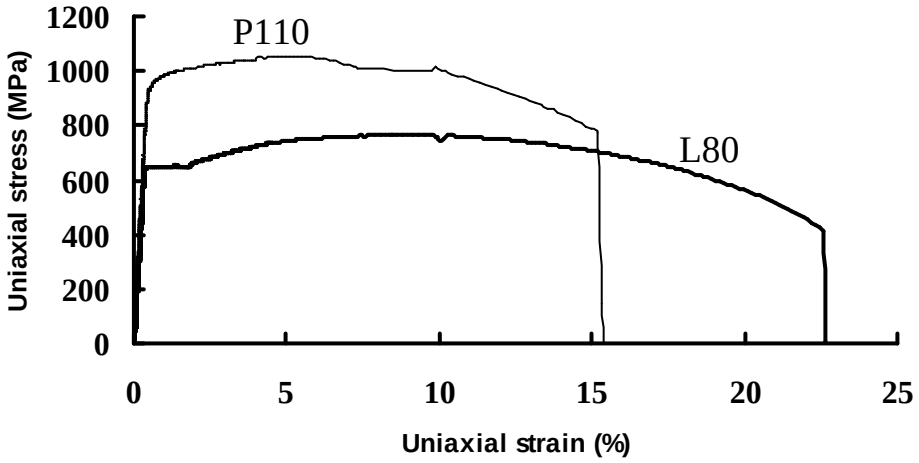

Figure 9

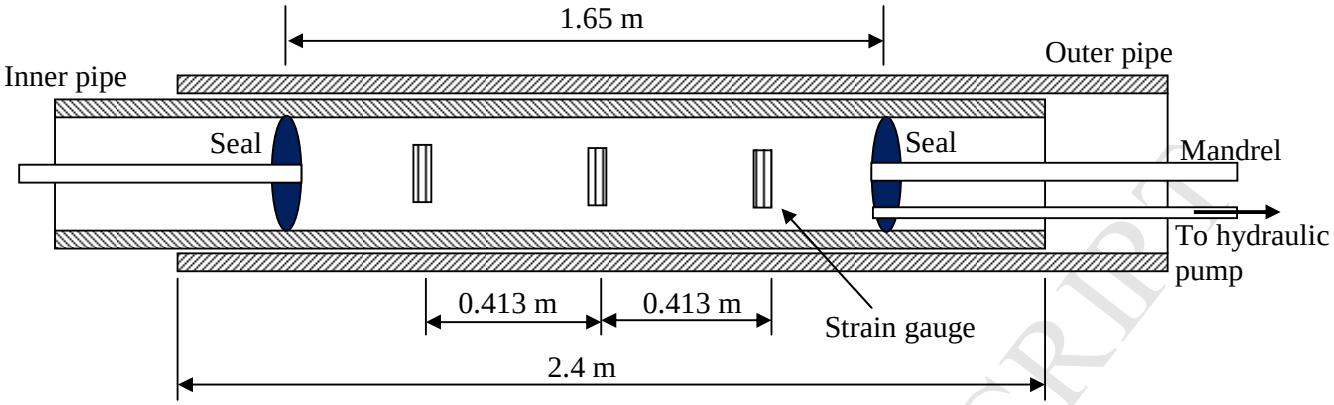

Figure 10

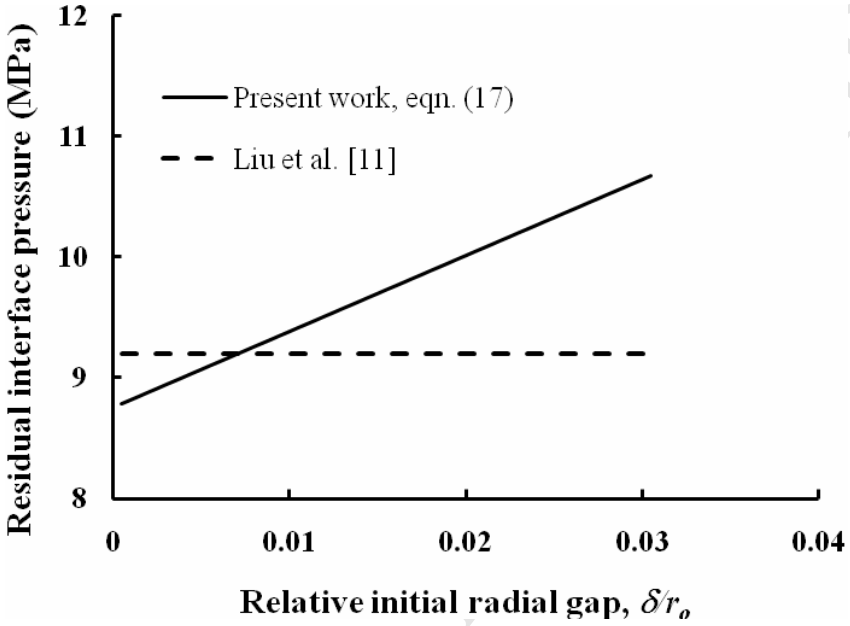

Figure 11